NANO LETTERS

Letter

pubs.acs.org/NanoLett

# Determination of the Thermal Noise Limit of Graphene Biotransistors

Michael S. Crosser,[†] Morgan A. Brown,[‡] Paul L. McEuen,[§] and Ethan D. Minot*[,‡]

[†]Department of Physics, Linfield College, McMinnville, Oregon 97128, United States

[‡]Department of Physics, Oregon State University, Corvallis, Oregon 97331, United States

[§]Kavli Institute at Cornell for Nanoscale Science, Cornell University, Ithaca, New York 14853, United States

Supporting Information

**ABSTRACT:** To determine the thermal noise limit of graphene biotransistors, we have measured the complex impedance between the basal plane of single-layer graphene and an aqueous electrolyte. The impedance is dominated by an imaginary component but has a finite real component. Invoking the fluctuation−dissipation theorem, we determine the power spectral density of thermally driven voltage fluctuations at the graphene/electrolyte interface. The fluctuations have $1/f^p$ dependence, with $p = 0.75-0.85$, and the magnitude of fluctuations scales inversely with area. Our results explain noise spectra previously measured in liquid-gated suspended graphene devices and provide realistic targets for future device performance.

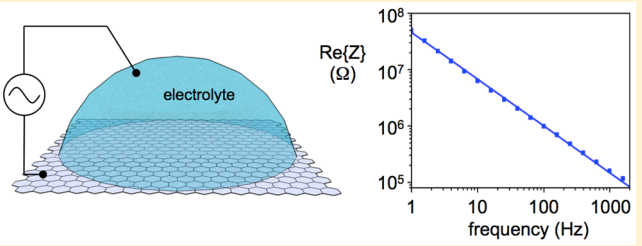


**KEYWORDS:** *Graphene field-effect transistor, noise, biosensor, 1/f noise, liquid gate*

Graphene field-effect transistors (GFETs) are a promising platform for many biosensing applications in liquid environments.[1] For example, extracellular voltages associated with action potentials cause a measurable change in the resistance of a GFET,[2,3] making GFETs attractive for neural recording techniques. The binding of charged molecules, such as proteins or DNA, can also be measured by GFET biosensors, making GFETs attractive for next-generation biomarker assays.[1]

The resolution of GFET sensors is typically limited by $1/f$ noise.[4] This noise can be traced to fluctuations in the carrier concentration, $n$, the carrier mobility, $\mu$, or both. For liquid-gated GFETs supported by an $SiO_2$ substrate, the dominant noise mechanism is the fluctuating occupancy of charge traps in the dielectric substrate which causes fluctuations in $n$.[5] This charge-trap $1/f$ noise can be reduced by removing the dielectric substrate and leaving the graphene suspended.[6] Additionally, "clean" dielectric materials such as hexagonal boron nitride[7] are likely to reduce charge-trap noise. As improvements in device design reduce charge-trap noise, it is important to determine the intrinsic limits set by thermal fluctuations that are present even in the cleanest devices. Knowledge of these fundamental limits is needed to set targets for device performance, and to develop a realistic vision of future applications.

In this work, we utilize the fluctuation−dissipation theorem to determine the thermally driven "liquid-gate Johnson noise" of GFET biosensors. Similar methodology has previously been employed to understand the Johnson noise measured from metal microelectrodes in contact with electrolytes.[8,9] Here we apply these ideas to liquid-gated transistors for the first time. First, we determine the frequency-dependent impedance between an aqueous electrolyte and a graphene sheet, $Z(f)$, for a number of different graphene devices. These measurements demonstrate that the graphene−electrolyte interface acts as a dissipative circuit element. This surprising result has important implications for biosensors as well as other systems, like graphene-based supercapacitors,[10] that utilize the graphene−electrolyte interface. After determining $Z(f)$, we use the fluctuation−dissipation theorem to predict the power spectral density of thermally driven voltage fluctuations across such a circuit element

$$S_{V,th}(f) = 4k_B T Z_{re}(f) \quad (1)$$

where $k_B$ is Boltzmann's constant, $T$ is temperature, and $Z_{re}(f)$ is the real component of the graphene−liquid impedance. This liquid-gate Johnson noise, $S_{V,th}(f)$, is distinct and independent from the Johnson noise associated with the channel-resistance of a GFET device. $S_{V,th}(f)$ varies with frequency and represents the lower limit for gate-voltage noise in liquid-gated GFETs.

Graphene on copper foil (ACS Materials) was transferred onto silicon wafers with a 300 nm oxide layer using a standard wet transfer procedure.[11] The graphene was patterned into squares of various dimensions via photolithography and $O_2$ plasma etching. To minimize the residue from photoresist,[12] a sacrificial layer of a polydimethyl glutarimide resist (LOR-3B from MicroChem Corporation) was deposited below the photoresist during each lithographic step. Source and drain contacts (2 nm Cr, 30 nm Au) were patterned via photolithography and electron beam evaporation (see Figure 1b).

**Received:** May 6, 2015
**Revised:** June 28, 2015





DOI: 10.1021/acs.nanolett.5b01788
*Nano Lett.* XXXX, XXX, XXX−XXX

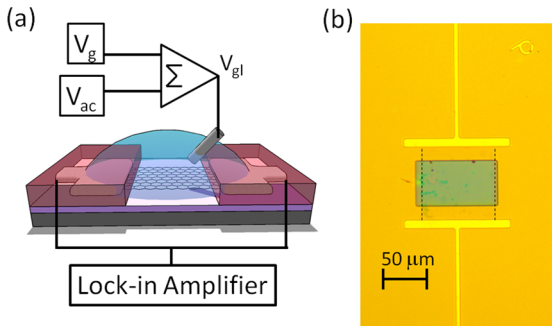


**Figure 1.** (a) Schematic of the impedance measurement: A dc voltage, $V_g$, and a small ac voltage, $V_{ac}$, are added together to define the liquid gate voltage $V_{gl}$. The ac component of the current, $I_{gl}$, is measured by the lock-in amplifier. (b) Optical microscope image of a device with an exposed graphene area of 5040 $\mu m^2$. Photoresist covers the remaining, visible surface. Dotted lines highlight the edges of the graphene.

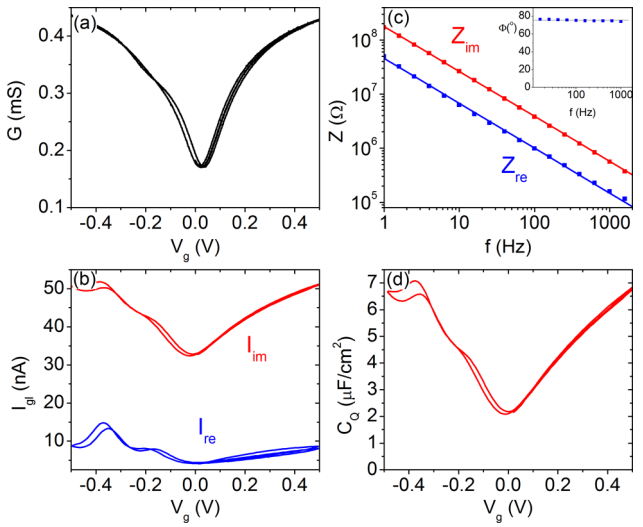


**Figure 2.** (a) Conductance of the graphene sheet as a function of liquid gate voltage. (b) Real and imaginary components of the graphene-to-liquid current measured at 1000 Hz. (c) $Z_{re}(f)$ and $Z_{im}(f)$ measured at $V_g = V_D$. The blue and red lines are fit using eq 2. Inset: phase angle of the complex impedance. (d) Quantum capacitance calculated from $|Z(1000\ \text{Hz})|$ as described in the main text.

To enable measurements of the electrolyte/graphene interface impedance, the metal electrodes were covered with an insulating layer of photoresist. Windows in the photoresist were patterned above the graphene (Figure 1). Devices were fabricated with various electrolyte/graphene contact areas (ranging from 3000 up to 23 000 $\mu m^2$). We also tested smaller devices, however, these tended to trap air bubbles inside the photoresist windows, rendering them unusable. One graphene device was left fully covered with photoresist so that parasitic capacitance between the liquid and the metal electrodes could be quantified (see Supporting Information).

We first characterized the devices by measuring direct current (dc) conductance between the source and drain electrodes (current flowing from metal to graphene to metal). A droplet of electrolyte was placed on the chip (10 mM phosphate buffer with pH 7.1). A small bias (25 mV) was applied to the source electrode and current was collected from the drain electrode. A dc gate voltage, $V_g$, was applied to the electrolyte solution using a tungsten wire with surface area much greater than that of the graphene device. Figure 2a shows a typical conductance curve $G(V_g)$. The conductance minimum has been shifted so as to occur at gate voltage $V_D \approx 0$, which we refer to as the Dirac point. The conductance characteristics are consistent with well-contacted high-quality graphene.

Next, a lock-in amplifier was used to investigate the impedance of the graphene-electrolyte interface. An alternating current (ac) perturbation, $(25\ \text{mV})\sin(2\pi ft)$, was added to $V_g$ via a summing circuit. The source and drain electrodes were shorted together and connected to a lock-in amplifier, allowing us to quantify the ac current flowing from the electrolyte into the graphene (Figure 1a).

Figure 2b shows the in-phase, $I_{re}$, and out-of-phase, $I_{im}$, components of the ac current passing through the graphene–electrolyte interface at $f = 1000$ Hz. Additional current due to the parasitic capacitance between the liquid and the metal leads has been subtracted ($I_{im}^{\text{parasitic}} = 23$ nA at 1000 Hz). For the graphene–electrolyte interface, $I_{im}$ is approximately 5 times larger than $I_{re}$.

The complex impedance of a double-layer capacitor (also known as an electrochemical capacitor) is commonly observed to be proportional to $1/(if)^p$, where $0 < p < 1$ and $i$ is the imaginary unit.[13] Expressing this complex impedance in terms of real and imaginary components gives

$$Z(f) \propto \frac{1}{f^p}\left(\cos\left(p\frac{\pi}{2}\right) - i\sin\left(p\frac{\pi}{2}\right)\right) \quad (2)$$

Interestingly, eq 2 predicts that a single parameter, $p$, can be used to fit both the constant phase angle, $\phi = \tan^{-1}(Z_{im}/Z_{re})$ and the exponent of the frequency dependence.

To compare our devices with eq 2, we measured $I_{re}$ and $I_{im}$ over a range of frequencies and calculated $Z_{re}$, $Z_{im}$, and $\phi$ (Figure 2c). We limit our analysis to the frequency range 1–1000 Hz, where the impedance of the double-layer capacitor dominates the response of the circuit. (A series resistance of less than 50 kΩ limits the flow of charge onto the double-layer capacitor at very high frequency. A parallel resistance of more than 1 GΩ, associated with electrochemical charge transfer, shunts the double-layer capacitor at very low frequency.) Coincidentally, 1–1000 Hz is the frequency range of interest for many biosensor applications. Figure 2c shows that a single fit parameter, $p = 0.83$, accurately describes both the constant $\phi$ and the power law relationship between $Z$ and $f$. Eight additional devices have been characterized and we consistently find good agreement with eq 2, with $p$ ranging from 0.75 to 0.85. This is the first report of constant $\phi < 90°$ for double-layer capacitors made from isolated single-layer graphene.

At $f = 1000$ Hz, the observed magnitude of the graphene-electrolyte impedance, $|Z|$, is consistent with previous work by Xia et al.[14] Xia et al. model the interface as two capacitances acting in series: (1) the quantum capacitance of the graphene, $C_Q$, which is proportional to the density of state at the Fermi level and therefore tunable by $V_g$, and (2) the capacitance of the ionic double layer, $C_{dl}$. For our experimental conditions, $C_{dl} \approx 16\ \mu\text{F/cm}^2$.[15] The total capacitance is then

$$C_{tot} = (C_{dl}^{-1} + C_Q^{-1})^{-1} \quad (3)$$

We equate $C_{tot}$ with the measured quantity $1/2\pi f|Z(f)|$ and use eq 3 to estimate $C_Q$ for our graphene devices (Figure 2d). The minimum value of $C_Q$ is 2 $\mu$F/cm$^2$, and the maximum slope is $|dC_Q/dV_g| = 18\ \mu\text{F/V}\cdot\text{cm}^2$. These values agree well with existing models for the density of states of single-layer graphene


DOI: 10.1021/acs.nanolett.5b01788
Nano Lett. XXXX, XXX, XXX–XXX

(see Supporting Information for further discussion). We conclude that our measurements at 1000 Hz exhibit the signatures of single-layer graphene but note that existing theory fails to explain $\phi < 90°$ and $|Z| \propto 1/f^p$.

Once $Z_{re}(f)$ is determined (Figure 2c), it is straightforward to apply eq 1 to predict the power spectral density of the voltage noise across the graphene/electrolyte interface, $S_{V,th}(f)$, which we term "liquid-gate Johnson noise" (Figure 3). Note

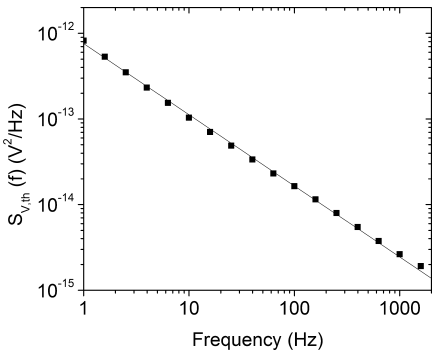


**Figure 3.** Predicted power spectral density of the liquid-gate Johnson noise, $S_{V,th}(f)$, for the device featured in Figure 2. Black squares are calculated from $Z_{re}(f)$ using eq 1. The fit line has frequency dependence $1/f^{0.83}$.

that the frequency dependence of $Z_{re}$ predicts a $1/f^p$ spectrum for the liquid-gate Johnson noise. This $1/f^p$ noise spectrum is strikingly different from the white noise that eq 1 predicts for an ideal resistor. It is interesting that the noise predicted by eq 1 can range from white noise to close to $1/f$ noise depending on the specific $Z_{re}(f)$ of the system.

We have measured $Z_{re}(f)$ for eight devices with a variety of sizes and gating conditions. These measurements are summarized in Figure 4, where we plot $S_{V,th}(1\ \text{Hz})$ for each device. For comparison, we also plot previously measured $S_V(1$ Hz) values obtained from time-domain measurements of the

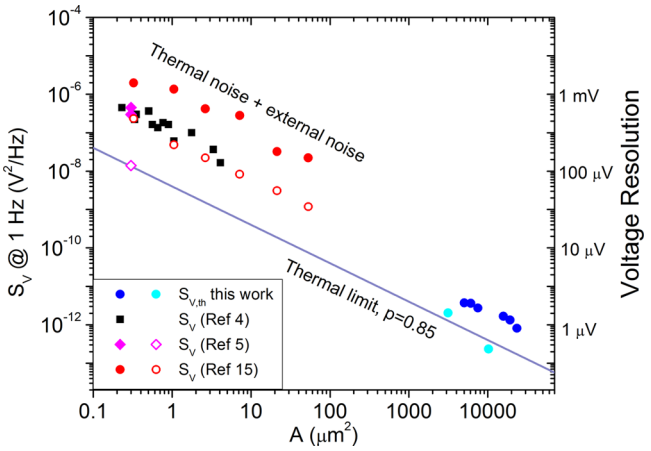


**Figure 4.** Plot of gate voltage noise power spectral density versus area for eight devices (this work), and a comparison with previous work on liquid-gated GFETs. The dark blue circles were measured with $V_g = V_D$. The light blue circles were measured at $V_g = V_D + 0.8$ V. The solid line with slope $A^{-1}$ shows our estimate for the thermal noise limit. For comparison, we plot the power spectral densities reported by other authors who measured similar GFET biosensors. Solid symbols correspond to GFET devices on oxide surfaces. Open symbols correspond to suspended GFET devices.

conductance fluctuations in GFETs (further discussion below). The right-hand axis of Figure 4 shows the equivalent voltage resolution, $V_{res}$, for a given value of $S_V$. We define $V_{res}$ as $(\int S_V(f)df)^{1/2}$ and use the approximation $V_{res} \simeq [S_V(1\ \text{Hz})(1\ \text{Hz})]^{1/2}$. This approximation is valid for a measurement bandwidth that spans one decade of frequency.

We first discuss the relationship between $S_{V,th}$ and the graphene surface area, $A$. As expected, we observe that $Z_{re}$ (and therefore $S_{V,th}$) scales inversely with $A$. Previous measurements of noise in GFETs,[5,6,16] and related systems such as metal electrodes,[8] show the same trend. The relationship $S_V \propto A^{-1}$ summarizes the trade-off between voltage resolution and spatial resolution.

Our results show that $S_{V,th}$ can be modified by gate voltage. Increasing $V_g$ adds carriers to the graphene and decreases both $Z_{im}$ and $Z_{re}$ with minimal change in $\phi$ (see Supporting Information). For highly doped graphene, $Z_{re}$ (and therefore $S_{V,th}$) is several times smaller than in lightly doped graphene. Using the highly doped values of $S_{V,th}$, we have estimated the "thermal noise limit" for graphene when $p = 0.85$ (solid line in Figure 4 with slope $A^{-1}$).

Our results are consistent with previous reports of gate voltage fluctuations in GFET biosensors. Previous measurements were sensitive to the sum of $S_{V,th}$ and extrinsic noise $S_{V,ext}$. We define the total noise power spectral density as

$$S_V = S_{V,th} + S_{V,ext} \quad (4)$$

where $S_{V,ext}$ is due to mechanisms such as the fluctuating occupancy of charge traps in the dielectric substrate. For GFETs on an $SiO_2$ substrate, $S_{V,ext}$ dominates the noise spectrum;[6] therefore, we expect $S_V > S_{V,th}$ for such devices (see Figure 4). In suspended GFETs (where the $SiO_2$ substrate has been removed) $S_V$ is reduced. Cheng et al.[6] report one device with $S_V$ equal to our estimated thermal noise limit (see Figure 4). The frequency dependence of the noise spectrum in Cheng's device, $1/f^{0.9}$, is consistent with eq 2 ($p < 1$). Other suspended GFET devices have been measured with $S_V > S_{V,th}$ (red open symbols in Figure 3).[16] These devices were likely "dirty" due to contact with mouse hearts (proteins and other biomolecules on the graphene surface contribute to $S_{V,ext}$[17]). We conclude that our work provides a framework for understanding the noise limit reached by clean suspended graphene FETs.

Finally, we comment on the performance of GFET biosensors compared to other materials. The thermally limited voltage resolution of GFET sensors is surprisingly similar to metal electrodes.[8,9] The measurements we report here elucidate the origin of this similarity. Both the graphene-electrolyte interface and the metal−electrolyte interface are imperfect capacitors. In both cases, the thermal noise is determined by $Z_{re}$, which is linked (via eq 2, and the parameter $p$) to the double-layer capacitance of an aqueous electrolyte in contact with a smooth conducting surface.

We conclude that standard GFET devices operating in liquid environments face voltage noise limits that are similar to those of metal electrodes. To reach lower noise levels, researchers will have to explore new ways of increasing $p$, the parameter describing the ideality of the double-layer capacitance. The microscopic mechanism responsible for $p < 1$ is currently not understood, therefore, future research into this mechanism has the potential to impact both biosensor applications as well as other applications that utilize graphene−electrolyte interfaces. Regardless of future efforts to increase $p$, GFET biosensors hold


DOI: 10.1021/acs.nanolett.5b01788
Nano Lett. XXXX, XXX, XXX−XXX

great promise. Graphene offers remarkable mechanical flexibility and biocompatibility, and in contrast to metal microelectrodes, FETs offer local amplification of weak signals. Local amplification is useful in applications such as neural recording where the signal-to-noise ratio can degrade during transmission to data acquisition hardware. With this strong set of properties, GFET devices are extremely promising for next-generation biosensors.

## ■ ASSOCIATED CONTENT

### Supporting Information

Control experiments to determine parasitic capacitance. Quantum capacitance of single-layer graphene. $Z(f)$ for devices of different area. Phase angle as a function of gate voltage. Source-drain current fluctuations caused by liquid-gate Johnson noise compared to fluctuations caused by channel-resistance Johnson noise. The Supporting Information is available free of charge on the ACS Publications website at DOI: 10.1021/acs.nanolett.5b01788.

## ■ AUTHOR INFORMATION

### Corresponding Author

*E-mail: ethan.minot@oregonstate.edu.

### Notes

The authors declare no competing financial interest.

## ■ ACKNOWLEDGMENTS

Funding for this research was provided by the National Science Foundation under award number DBI-1450967.

## ■ REFERENCES

(1) Liu, Y.; Dong, X.; Chen, P. *Chem. Soc. Rev.* **2012**, *41* (6), 2283−2307.
(2) Cohen-karni, T.; Qing, Q.; Li, Q. L.; Fang, Y.; Lieber, C. M. *Nano Lett.* **2010**, *10*, 1098.
(3) Hess, L. H.; Jansen, M.; Maybeck, V.; Hauf, M. V.; Seifert, M.; Stutzmann, M.; Sharp, I. D.; Offenhausser, A.; Garrido, J. A. *Adv. Mater.* **2011**, *23*, 5045.
(4) Balandin, A. *Nat. Nanotechnol.* **2013**, *8* (8), 549−555.
(5) Heller, I.; Chatoor, S.; Männik, J.; Zevenbergen, M. a G.; Oostinga, J. B.; Morpurgo, A. F.; Dekker, C.; Lemay, S. G. *Nano Lett.* **2010**, *10* (5), 1563−1567.
(6) Cheng, Z.; Li, Q.; Li, Z.; Zhou, Q.; Fang, Y. *Nano Lett.* **2010**, *10* (5), 1864−1868.
(7) Petrone, N.; Dean, C. R.; Meric, I.; van der Zande, A. M.; Huang, P. Y.; Wang, L.; Muller, D.; Shepard, K. L.; Hone, J. *Nano Lett.* **2012**, *12* (6), 2751−2756.
(8) Gesteland, R.; Howland, B.; Lettvin, J. Y.; Pitts, W. H. *Proc. IRE* **1959**, *47* (11), 1856−1959.
(9) Robinson, D. A. *Proc. IEEE* **1968**, *56* (6), 1065−1071.
(10) Stoller, M. D.; Park, S.; Zhu, Y.; An, J.; Ruoff, R. S. *Nano Lett.* **2008**, *8*, 6−10.
(11) Saltzgaber, G.; Wojcik, P.; Sharf, T.; Leyden, M. R.; Wardini, J. L.; Heist, C. a; Adenuga, A. a; Remcho, V. T.; Minot, E. D. *Nanotechnology* **2013**, *24* (35), 355502.
(12) Lerner, M. B.; Matsunaga, F.; Han, G. H.; Hong, S. J.; Xi, J.; Crook, A.; Perez-Aguilar, J. M.; Park, Y. W.; Saven, J. G.; Liu, R.; Johnson, a T. C. *Nano Lett.* **2014**, *14* (5), 2709−2714.
(13) Kötz, R.; Carlen, M. *Electrochim. Acta* **2000**, *45*, 2483−2498.
(14) Xia, J.; Chen, F.; Li, J.; Tao, N. *Nat. Nanotechnol.* **2009**, *4* (8), 505−509.
(15) Rieger, P. *Electrochemistry*, 2nd ed.; Chapman & Hall: New York, 1994.
(16) Cheng, Z.; Hou, J.; Zhou, Q.; Li, T.; Li, H.; Yang, L.; Jiang, K.; Wang, C.; Li, Y.; Fang, Y. *Nano Lett.* **2013**, *13* (6), 2902−2907.
(17) Sharf, T.; Kevek, J. W.; Deborde, T.; Wardini, J. L.; Minot, E. D. *Nano Lett.* **2012**, *12* (12), 6380−6384.



DOI: 10.1021/acs.nanolett.5b01788
*Nano Lett.* XXXX, XXX, XXX−XXX